Application of the fractional Fourier transformation to digital holography recorded by an elliptical and astigmatic Gaussian beam

E. Nicolas, S. Coëtmellec, M. Brunel, D. Allano and D. Lebrun †

A.J.E.M Janssen ‡

†Groupe d'Optique et d'Optoélectronique, UMR-6614 CORIA, Av. de l'Université, 76801 Saint-Etienne du Rouvray cedex, France,

‡Philips Research Laboratories-Building WO-02, Prof. Holstlaan 4, 5656 AA Eindhoven, The Netherlands

coetmellec@coria.fr, a.j.e.m.janssen@philips.com

Abstract: In this paper, we demonstrate that the fractional Fourier transformation yields a suitable method to analyze the diffraction patterns produced by a particle field illuminated by an astigmatic and elliptical Gaussian beam. Simulations and experimental results are presented.

OCIS codes: 090.0090, 070.0070, 100.0100

1. Introduction

In many studies of digital in-line holography (DIH), the incident beam which illuminates the particles is considered as a homogeneous and collimated plane wave. But, two problems appear in such a simple optical configuration. First, the metrology by microscopy on small particles is not possible because a diverging beam must be used and, second by, it also appears that in most experimental cases, the beam is Gaussian, elliptical

and astigmatic because laser diode sources are more and more used to illuminate the particles. As a result the intensity distribution on the image detector is distorted and the quality of the reconstructed particle image is deteriorated. Moreover, the resolution in the horizontal or vertical direction is affected by the astigmatism.[11] The holographic images can be reconstructed by means of popular mathematical tools such as the wavelet transformation[3, 7, 19] or the Fresnel transformation.[14] Gustafsson *et al.* used the Rayleigh-Sommerfeld diffraction integral. However, these classical integral transformations cannot be rigourously applied to reconstruct particle holograms that have been recorded by means of an elliptic and astigmatic Gaussian beam because the astigmatism is not taken into account in the kernel of such integrals. Recently, the two-dimensional fractional Fourier transformation (FRFT) has been advantageously used to reconstruct in-line holograms of particle fields.[10, 23] Many papers deal with the propagation of an elliptical Gaussian beam through a paraxial system.[8, 20] More recently, a study of the fractional Fourier transform of an elliptical Gaussian beam has been developed.[9] However these studies never consider the phenomenon of diffraction by an object.

In the present publication we show that the 2D FRFT can be used to reconstruct particle holograms recorded with elliptic astigmatic beams. In Section 2, we first give a solution to calculate the diffraction pattern produced by a circular particle illuminated by an elliptical and astigmatic Gaussian beam by applying a method of decomposition on the Zernike bases. These results allow us to simulate the diffraction patterns that are necessary in Section 3. In this Section 3, we recall the definition of the two-dimensional FRFT and we show that this tool enables us to reconstruct such particle holograms. The elliptical properties of the recording beam are taken into account by an appropriate adjustment of the fractional orders along x-axis and y-axis. Experimental results are also presented.

2. In-Line Holography with an elliptic and astigmatic Gaussian beam

Let us recall the intensity distribution recorded by in-line holograms. Let $1-T(\xi,\eta)$ be the amplitude transmission function of the object to be recorded. This object is supposed to be illuminated by a monochromatic electromagnetic wave that propagates through a linear, nondispersive, isotropic and homogeneous medium. The object is supposed to be a perfectly absorbing particle located at a distance z from a quadratic sensor along the optical axis. In this publication, we only consider the particular case where the object is centered on the propagation axis. Under Fresnel approximation, the Huygens-Fresnel diffraction formula is given by

the scalar integral:

$$A(x,y) = \frac{\exp(i\frac{2\pi}{\lambda}z)}{i\lambda z}\int_{-\infty}^{+\infty}\int_{-\infty}^{+\infty} E(\xi,\eta)\,[1-T(\xi,\eta)]\,\exp\left(\frac{i\pi}{\lambda z}\left[(\xi-x)^2+(\eta-y)^2\right]\right)d\xi\,d\eta\,, \tag{1}$$

where λ is the wavelength and $A(x,y)$ is the complex amplitude in the quadratic sensor plane. The $\exp(i\frac{2\pi}{\lambda}z)$ thereafter term will be omitted . For an opaque disk of diameter d and centered at the origin O, the transmittance function $T(\xi,\eta)$ in the object plane is:

$$T(\xi,\eta) = \begin{cases} 1 & \text{if } \sqrt{\xi^2+\eta^2} < \mathrm{d}/2, \\ 1/2 & \text{if } \sqrt{\xi^2+\eta^2} = \mathrm{d}/2, \\ 0 & \text{otherwise.} \end{cases} \tag{2}$$

If we assume that this object is illuminated by an elliptic and astigmatic Gaussian beam, the expression for $E(\xi,\eta)$ is, up to a proportionality factor, given by

$$E(\xi,\eta) = \exp\left(-\left[\frac{\xi^2}{\omega_\xi^2}+\frac{\eta^2}{\omega_\eta^2}\right]\right)\exp\left(-i\frac{\pi}{\lambda}\left[\frac{\xi^2}{R_\xi}+\frac{\eta^2}{R_\eta}\right]\right) \tag{3}$$

R_q with $q=\xi,\eta$ are the wavefront curvatures and ω_q denote the beam widths along the ξ-axis and η-axis. These four parameters are defined in the object plane. To calculate the integral of the Eq.(1), $A(x,y)$ is split it into two integrals:

$$A_1(x,y) = \int_{-\infty}^{+\infty}\int_{-\infty}^{+\infty} E(\xi,\eta)\,\exp\left(\frac{i\pi}{\lambda z}\left[(\xi-x)^2+(\eta-y)^2\right]\right)d\xi\,d\eta, \tag{4}$$

and

$$A_2(x,y) = \int_{-\infty}^{+\infty}\int_{-\infty}^{+\infty} E(\xi,\eta)\,T(\xi,\eta)\,\exp\left(\frac{i\pi}{\lambda z}\left[(\xi-x)^2+(\eta-y)^2\right]\right)d\xi\,d\eta\,, \tag{5}$$

so that

$$A(x,y) = \frac{1}{i\lambda z}\left[A_1(x,y)-A_2(x,y)\right]. \tag{6}$$

A. Expression for $A_1(x, y)$

The development of Eq.(4) gives us:

$$A_1(\mathbf{r}) = K(\omega_\xi, R_\xi)K(\omega_\eta, R_\eta)\exp\left(-\frac{\pi}{\lambda z}\mathbf{r}^{\mathrm{T}}N\mathbf{r}\right)\exp\left(i\frac{\pi}{\lambda z}\mathbf{r}^{\mathrm{T}}M\mathbf{r}\right) \tag{7}$$

where $\mathbf{r}^{\mathrm{T}}$ represents the vector $(x \quad y)$, $A_1(\mathbf{r})$ denotes the value of A_1 at the point (x, y), and the factors $K(\omega_q, R_q)$ in Eq.(7) are defined by

$$K(\omega_q, R_q) = \left(\frac{\pi\omega_q^2}{1 + i\frac{\pi\omega_q^2}{\lambda z}\left(\frac{z}{R_q} - 1\right)}\right)^{1/2}. \tag{8}$$

The matrices N and M:

$$N = \begin{pmatrix} N_x & 0 \\ 0 & N_y \end{pmatrix}, \qquad M = \begin{pmatrix} M_x & 0 \\ 0 & M_y \end{pmatrix}, \tag{9}$$

with

$$N_q = \frac{\pi}{\lambda z}\,\frac{\omega_q^2}{1 + \frac{\pi^2}{\lambda^2}\omega_q^4\left(\frac{1}{R_q} - \frac{1}{z}\right)^2} \qquad , \qquad M_q = 1 + \frac{\pi}{\lambda z}\,\frac{\omega_q^4\,\frac{\pi}{\lambda}\left(\frac{1}{R_q} - \frac{1}{z}\right)}{1 + \frac{\pi^2}{\lambda^2}\omega_q^4\left(\frac{1}{R_q} - \frac{1}{z}\right)^2}, \tag{10}$$

are introduced here to simplify the equations.

B. Expression for $A_2(x, y)$

For the calculation of $A_2(x, y)$, Nijboer-Zernike theory and the results for the diffraction integral in the presence of aberrations can be used.[5] To do that, it is convenient here to restate $A_2(x, y)$ in cylindrical coordinates as follows: $\xi = d\sigma\cos(\varphi)/2$ and $\eta = d\sigma\sin(\varphi)/2$ for the object plane. In the sensor plane, $x = r\cos\theta$, $y = r\sin\theta$. Considering these substitutions in Eqs.(2) and (5), we obtain:

$$A_2(r, \theta) = \frac{d^2}{4}\exp\left(i\frac{\pi r^2}{\lambda z}\right)\cdot\int_0^1\int_0^{2\pi}\exp\left(-a\sigma^2 + b\sigma^2\cos 2\varphi\right)\exp\left(-i\frac{\pi d}{\lambda z}r\sigma\cos(\varphi - \theta)\right)\sigma\, d\sigma\, d\varphi \tag{11}$$

with

$$\begin{cases} a = \dfrac{d^2}{4}\,a_1 + i\pi\dfrac{d^2}{4}\left(b_1 - \dfrac{1}{\lambda z}\right), \qquad b = \dfrac{d^2}{4}\,a_2 + i\pi\dfrac{d^2}{4}b_2, \\ a_1 = \dfrac{1}{2}\left(\dfrac{1}{\omega_\xi^2} + \dfrac{1}{\omega_\eta^2}\right), \qquad a_2 = \dfrac{1}{2}\left(\dfrac{1}{\omega_\xi^2} - \dfrac{1}{\omega_\eta^2}\right), \\ b_1 = \frac{1}{2\lambda}\left(\frac{1}{R_\xi} + \frac{1}{R_\eta}\right), \qquad b_2 = \frac{1}{2\lambda}\left(\frac{1}{R_\xi} - \frac{1}{R_\eta}\right). \end{cases} \tag{12}$$

$A_2(r,\theta)$ can be rewritten as the following series:[5]

$$A_2(r,\theta) = \pi d^2 \exp\left(i\frac{\pi r^2}{\lambda z}\right) \sum_{k=0}^{\infty} (-i)^k \varepsilon_k \, T_k(r) \cos(2k\theta) \tag{13}$$

with $\varepsilon_k = 1/2$ if $k = 0$ and 1 otherwise. $T_k(r)$ is defined as:

$$T_k(r) = \int_0^1 \exp\left(i\frac{1}{2}u\sigma^2\right) J_k(\gamma_2\,\sigma^2) J_{2k}\left(\frac{\pi d}{\lambda z} r\sigma\right) \sigma d\sigma, \tag{14}$$

where

$$\begin{aligned} u &= \frac{\pi d^2}{2\lambda z}(-1 + \lambda z b_1) - i a_1 \frac{d^2}{2}, \\ \gamma_2 &= \frac{d^2}{4}(-\pi b_2 + i a_2). \end{aligned} \tag{15}$$

It must be noted that $T_k(r)$ will be considered in the next section for the calculation of the fractional Fourier transform of the intensity distribution in the diffraction pattern. Thus the product of the domain and fractional domain sampling interval must be a function of the fractional order.[21] This property is linked to the chirp functions used in the fractional operator. Consequently, to properly evaluate $T_k(r)$, that contains a linear chirp term ($\frac{1}{2}u\sigma^2$) too, it is necessary to rewrite $T_k(r)$ as the following non-integral form:

$$T_k(r) = \sum_{p=0}^{\infty} \beta_{2k+2p}^{2k}(\gamma_2) V_{2k+2p}^{2k}(r,u), \tag{16}$$

where the coefficient $\beta_{2k+2p}^{2k}(\gamma_2)$ and $V_{2k+2p}^{2k}(r,u)$ are given by the analytical development of $T_k(r)$ in Appendix A. In Eq. (14) the first Bessel function has $\gamma_2\sigma^2$ rather than σ as argument. Consequently, the method of Nijboer-Zernike and Bauer's identity cannot be used to simplify the solution (see Ref.,[5] p. 534). Furthermore, note that the parameter γ_2 is linked to the astigmatism of the Gaussian beam. Indeed, in the particular case where the beam is circular, we have $\gamma_2 = 0$. Then the first Bessel function is equal to zero for all values of $k > 0$. For $k = 0$, the Bessel function is unity and by using Bauer's identity (with $u \neq 0$), we recover the special case of an aberration-free wave.[5]

From the Eqs. (6), (7) and (13), the intensity distribution of the diffraction pattern, denoted by $I(x,y)$, can be evaluated as:

$$I(x,y) = A(x,y)A^*(x,y), \tag{17}$$

where * denotes the complex conjugate. As the aim is to reconstruct the image of the particle by means of the fractional Fourier transformation from intensity distribution of the diffraction pattern $I(x,y)$, the

next section is devoted to recall the definition of the FRFT and gives the method for having a reliable reconstruction of a particle image.

3. Fractional Fourier transformation analysis of in-line holograms

A. Two-dimensional Fractional Fourier transformation

The FRFT is a generalization of the classical Fourier transformation. Its mathematical definition is as follows:[15,16,18] the two-dimensional fractional Fourier transformation of order a_x for x-cross-section and a_y for y-cross-section with $0 \leq |\alpha_x| \leq \pi/2$ and $0 \leq |\alpha_y| \leq \pi/2$, respectively, is defined as (with $\alpha_p = \frac{a_p \pi}{2}$)

$$\mathscr{F}_{\alpha_x,\alpha_y}[I(x,y)](x_a,y_a) = \int_{\mathbb{R}^2} N_{\alpha_x}(x,x_a)\, N_{\alpha_y}(y,y_a) I(x,y)\, dx\, dy \tag{18}$$

where the kernel of the fractional operator is defined by

$$N_{\alpha_p}(x,x_a) = C(\alpha_p) \exp\left(i\pi \frac{x^2+x_a^2}{s^2 \tan\alpha_p}\right) \exp\left(-\frac{i2\pi x_a x}{s^2 \sin\alpha_p}\right), \tag{19}$$

and

$$C(\alpha_p) = \frac{\exp(-i(\frac{\pi}{4}\mathrm{sign}(\sin\alpha_p) - \frac{\alpha_p}{2}))}{|s^2 \sin\alpha_p|^{1/2}}. \tag{20}$$

Here $p = x, y$. s is an arbitrary fixed scaling parameter and has the dimension of distance. The energy-conservation law is ensured by the coefficient $C(\alpha_p)$ which is a function of the fractional order . Now recall the main properties. $\mathscr{F}_{\pi/2,\pi/2}$ is the ordinary Fourier transformation and $\mathscr{F}_{0,0}$ is the identity operator.

B. Reconstruction: optimal fractional orders

In many digital reconstruction studies, the Huygens-Fresnel integral is expressed as a convolution operation. This formulation simplifies the computation of this integral by realizing a simple product in the spectral domain by means of the fast Fourier transformation (FFT) algorithm. In the same way, the reconstruction process of a hologram can be expressed as a convolution between the transmission function of a holographic plate and the Fresnel kernel $h_z(x,y)$ taking the form[7]

$$h_z(x,y) = \frac{1}{i2\pi} \exp\left(i\frac{\pi}{\lambda z}(x^2+y^2)\right). \tag{21}$$

It should be noted that applying such a method poses a problem because the two-dimensional convolution kernel is a chirp-like function. Therefore, its Fourier transformation is also a chirp function. Moreover, h_z

is not well adapted to analyse both x and y linear chirps at the same time (*i.e.* curvatures R_ξ and R_η) to reconstruct the image of the particles. But this can be achieved with the fractional Fourier transformation. The reconstruction process is decomposed into two steps: the first step consists in removing the linear chirp along the x-axis and along the y-axis contained in the intensity distribution of the diffracted field by applying a fractional Fourier transformation with the optimal fractional orders, noted α_x^{opt} and α_y^{opt}. The second step is to apply a standard Fourier transformation.

In order to realize this numerical reconstruction, we first have to determine the phase contained in the intensity distribution of the diffraction pattern of the particle. This analysis is possible by using with the analytical development presented in the previous section:

$$I(x,y) = A(x,y)A^*(x,y) = \kappa\left(|A_1|^2 + |A_2|^2\right) - 2\kappa\,\Re\left\{A_1 A_2^*\right\} \tag{22}$$

$\Re$ denotes the real part and $\kappa = 1/(\lambda z)^2$ is a constant which is not important in the present study. $\kappa|A_1|^2$ corresponds to the directly transmitted Gaussian light. Note that if $\omega_\xi = \omega_\eta = \omega$ and $R_\xi = R_\eta = R$ then

$$\lim_{\substack{\omega\to\infty \\ R\to\infty}} \kappa|A_1|^2 = 1.$$

This limit corresponds to the first term of the Eqs. (12) or (13) of [10]. In the same way, the second term, in the Fresnel approximation, takes the following form:

$$\lim_{\substack{\omega\to\infty \\ R\to\infty}} \kappa|A_2|^2 = U_1^2\left(\frac{\pi d^2}{2\lambda z}, \frac{\pi d}{\lambda z}r\right) + U_2^2\left(\frac{\pi d^2}{2\lambda z}, \frac{\pi d}{\lambda z}r\right) \simeq \frac{1}{(\lambda z)^2}\left(\frac{\pi d^2}{2}\right)^2 \frac{J_1^2(\frac{\pi d}{\lambda z}r)}{(\frac{\pi d}{\lambda z}r)^2}, \tag{23}$$

where U_1 and U_2 are the Lommel functions (see Ref. [5], p. 487). The right hand side expression of Eq. (23) corresponds to the far-field approximation, *i.e.* $\pi d^2/2\lambda z \ll 1$, on the Lommel's functions. This term is defined by the Fourier transform of the object function. Again we obtain the third term of the Eq. (13) of [10]. Finally, if the same treatment is realized of the third term of the Eq. (22), one has the following limit:

$$\lim_{\substack{\omega\to\infty \\ R\to\infty}} 2\kappa\,\Re\left\{A_1 A_2^*\right\} \simeq \frac{\pi d^2}{\lambda z}\sin\left(\frac{\pi r^2}{\lambda z}\right)\frac{J_1(\frac{\pi d}{\lambda z}r)}{(\frac{\pi d}{\lambda z}r)}. \tag{24}$$

$2\kappa\Re\left\{A_1 A_2^*\right\}$ is the most important term and corresponds to a modulation of the linear chirp function modulated by sum of Bessel functions $T_k(r)$. The linear chirp is inversely proportional to the recording distance z while $T_k(r)$ is also linked to the diameter of the particle. This modulation creates the interference pattern recorded by the CCD which enables the reconstruction of the real image. As we have seen before, the

method adopted here is to remove a quadratic phase contained in $\Re\{A_1 A_2^*\}$ to reconstruct the image of the particle and to localize it in the space. The quadratic phase is denoted $\varphi(x,y)$ and its analytical expression can be determine from Eqs. (7) and (13). Firstly, from Eq. (22) we write

$$A_1 A_2^* = |A_1 A_2^*| \exp\left(i\varphi(x,y)\right) \tag{25}$$

where

$$\varphi(x,y) = -\frac{\pi}{\lambda z}\left(x^2(M_x - 1) + y^2(M_y - 1)\right). \tag{26}$$

M_x, M_y are given in the Eqs. (9) and (10). The quadratic phase of the kernel of the FRFT denoted by $\varphi_a(x,y)$ is

$$\varphi_a(x,y) = \frac{\pi}{s^2}\left(x^2 \cot\alpha_x + y^2 \cot\alpha_y\right). \tag{27}$$

Now to reconstruct the image of the particle, the following transformation must be calculated:

$$\begin{aligned}\mathscr{F}_{\alpha_x,\alpha_y}[I(x,y)](x_a,y_a) = \kappa\mathscr{F}_{\alpha_x,\alpha_y}\left[|A_1|^2 + |A_2|^2\right](x_a,y_a) - \\ 2\kappa\mathscr{F}_{\alpha_x,\alpha_y}\left[|A_1 A_2^*|\cos(\varphi(x,y))\right](x_a,y_a)\end{aligned} \tag{28}$$

The first term is uninteresting and does not allow us to reconstruct the particle image. Only the second term will be considered for the image reconstruction.[10] By noting that $2\cos\varphi = \exp(-i\varphi) + \exp(i\varphi)$, Eq. (28) becomes :

$$\begin{aligned}\mathscr{F}_{\alpha_x,\alpha_y}[I(x,y)](x_a,y_a) = \kappa\mathscr{F}_{\alpha_x,\alpha_y}\left[|A_1|^2 + |A_2|^2\right](x_a,y_a) \\ - \kappa C(\alpha_x)C(\alpha_y)\int_{\mathbb{R}^2} |A_1 A_2^*| \exp\left(i(\varphi_a - \varphi)\right)\exp\left(-\frac{i2\pi}{s^2}\left(\frac{x_a x}{\sin\alpha_x} + \frac{y_a y}{\sin\alpha_y}\right)\right) dx\,dy \\ - \kappa C(\alpha_x)C(\alpha_y)\int_{\mathbb{R}^2} |A_1 A_2^*| \exp\left(i(\varphi_a + \varphi)\right)\exp\left(-\frac{i2\pi}{s^2}\left(\frac{x_a x}{\sin\alpha_x} + \frac{y_a y}{\sin\alpha_y}\right)\right) dx\,dy.\end{aligned} \tag{29}$$

The reconstruction of an image is archieved when one of the quadratic phase terms under the integral operator $\mathscr{F}_{\alpha_x,\alpha_y}$, is equal to zero, *i.e.*:

$$\varphi_a(x,y) \pm \varphi(x,y) = 0. \tag{30}$$

The first solution $\varphi_a - \varphi = 0$ corresponds to the reconstruction of the real image while $\varphi_a + \varphi = 0$ leads to reconstruction of the virtual image. The first case is realized by choosing the positive optimal fractional

orders α_x^{opt} and α_y^{opt}. Their explicit expression can be determined from Eqs. (26) and (27).

$$\tan\alpha_x^{opt} = -\frac{\lambda z}{s^2(M_x-1)} \qquad \tan\alpha_y^{opt} = -\frac{\lambda z}{s^2(M_y-1)}. \tag{31}$$

The second case is realized by choosing the negative fractional orders $-\alpha_x^{opt}$ and $-\alpha_y^{opt}$. Finally, the optimal fractional orders allow us to reconstruct the image of the particle using a standard Fourier transformation. For infinite values of R_q and ω_q (particular case of an homogeneous plane wave), Eq. (35) of Ref. [10] is recovered.

C. Numerical experiments

The simulations are realized in the experimental context presented by the Fig. (1). The diameter of original and circular beam width in front of the cylindric lense (CL) is $2\omega = 14mm$ and the particle is located at a distance $\delta = 250mm$ from CL. The focal lengths f_q of the cylindrical lens are infinite along an axis parallel to the ξ-axis and equal to $200mm$ along an axis parallel to the η-axis. The wavelength of the laser beam is $\lambda = 632.8nm$. From theses four characteristics of the beam, the numerical values (R_ξ, R_η, ω_ξ and ω_η from the Eq. (3)) which describe the geometry of the beam in the plane of the particle are determined by a straightforward analytical development of the Fresnel integral applied to a circular Gaussian function :

$$\omega_q = \frac{\lambda\delta}{\pi\omega}\left(1+\left(\frac{\pi\omega^2}{\delta\lambda}\right)^2\left(\frac{\delta}{f_q}-1\right)^2\right)^{1/2} \qquad \text{and} \qquad R_q = -\frac{\delta}{1+\frac{\left(\frac{\pi\omega^2}{\delta\lambda}\right)^2\left(\frac{\delta}{f_q}-1\right)}{1+\left(\frac{\pi\omega^2}{\delta\lambda}\right)^2(\frac{\delta}{f_q}-1)^2}}. \tag{32}$$

Figure 2 illustrates an application of this model by a simulation of the diffraction pattern resulting from a particle with a diameter $d = 150\mu m$ illuminated by an elliptical and astigmatic Gaussian beam and localized at $z = 145mm$ from the CCD camera. By using Eq. (32), the characteristics of the Gaussian beam in the object plane are $\omega_\xi = 7mm$, $\omega_\eta = 1.75mm$, and curvatures radius are $R_\xi = -2.36\cdot 10^5 m$, $R_\eta = -50mm$. The analytical expression developed in Section 2 has been used to calculate the intensity distribution in a diffraction pattern recorded by means of an elliptic beam. As a result, knowing the beam parameters, the optimal fractional orders can be easily calculated and used for image reconstruction.

Now, consider the diffraction pattern represented in Fig. (2) of a $150\mu m$ particle located at distance $z = 107mm$ from the CCD camera. Recall that the characteristics of the Gaussian beam in the plane of the

particle are $\omega_\xi = 7mm$, $\omega_\eta = 1.75mm$, and curvatures are defined by $R_\xi = -2.36 \cdot 10^5 m$ and $R_\eta = -50mm$. The optimal fractional orders obtained from the relations (31) are:

$$a_x^{opt} = 0.521 \qquad a_y^{opt} = 0.816. \tag{33}$$

The reconstructed particle image with the fractional Fourier transformation is shown in Fig. (3). As we can see, a circular particle image has been retrieved from a noncircular symmetric diffraction pattern. This particle image could not have been obtained with the conventional methods such as Fresnel or Fraunhofer transformations. Indeed the quadratic phase term of the Fresnel integral kernel defined by Eq. (21) cannot accommodate the condition imposed by Eq. (30) and therefore is unsuited to reconstruct particle images.

Another particular case merits to be presented in order to complete our argumentation on the advantages of using the fractional Fourier transformation. Let us consider a particular case of the diffraction pattern represented in Fig. (4). In this example, $\delta = 135mm$ and $z = 154mm$. Such a hyperbolic shape of the diffraction pattern results from a singular location of the particle ($d = 150\mu m$). This situation occurs when the object is placed between the cylindric lens (CL) and the beam waist. In this case, R_ξ and R_η have opposite signs. From Eq. (32), we find $\omega_\xi = 7mm$, $\omega_\eta = 2.27mm$, $R_\xi = -4.38 \cdot 10^5 m$ and $R_\eta = 65mm$ for the characteristics of the Gaussian beam in the object plane. These values allow us to determine the optimal fractional orders by means of Eq. (31):

$$a_x^{opt} = 0.633 \qquad a_y^{opt} = -0.718. \tag{34}$$

The particle image reconstructed with these fractional orders is represented in Fig. (5). Here again, a circular shape of the particle image is recovered. In both cases (Figs. (3), (5)) background fringes, that appear around the images, are due to the so-called twin image usually observed in Gabor holography.

D. Experimental results

In order to validate the above method to a practical case, we have used an experimental setup where the beam parameters are close to the parameters used in the previous subsection. Here, a He-Ne laser of wavelength equal to $632.8nm$ is used. And a $150\mu m$ opaque disk localized at $z = 106mm$ is illuminated by an elliptical Gaussian beam with the widths $\omega_\xi = 7mm$, $\omega_\eta = 1.75mm$. The curvatures along each axis are $R_\xi = -2.36 \cdot 10^5 m$ and $R_\eta = -50mm$. The pixel size of the CCD camera is equal to $11\mu m$. The diffraction

pattern recorded by this camera is illustrated in Fig. (6). The optimal fractional orders deduced from the previous parameters are equal to: $a_x^{opt} = 0.518$ and $a_y^{opt} = 0.813$. Figure 7 shows the reconstruction of the object field from the Fig. (6).

Secondly, we have computed the reconstruction of a $150\mu m$ particle diameter illuminated by the same Gaussian beam but located between CL and the beam waist. Here, the beam widths are $\omega_\xi = 7mm$, $\omega_\eta = 2.27mm$ and the curvatures along each axis are $R_\xi = -4.38 \cdot 10^5 m$ and $R_\eta = 65mm$. The diffraction pattern recorded by this camera is illustrated in Fig. (8). The optimal fractional orders deduced from the previous parameters are equal to: $a_x^{opt} = 0.633$ and $a_y^{opt} = -0.718$. Figure 9 shows the reconstructed object field. The straight fringes observed in both sides of the Fig. (7) and (9) are due to the Gibbs phenomenon and are close to the signal reconstruction from amplitude in Ref. [2]. The experimental results presented in this subsection show that the particle images are well reconstructed with a high contrast.

4. Conclusion

In this paper we have proposed an analytical solution of scalar diffraction of an elliptical and astigmatic Gaussian beam by an opaque disk under Fresnel approximation. For two examples a good agreement between the simulated intensity distributions and experimental results has been demonstrated. Such a diffraction pattern cannot be directly analyzed by Fresnel integral and therefore cannot lead to a satisfactory image reconstruction. However, using the fractional Fourier transformation allows us a good particle image reconstruction. Again, this presents a strong advantage as regards to classic methods based on the convolution product where three FFT and a multiplication must be realized before reconstructing the object field.

A Appendix A : Analytical development of $T_k(r)$

To develop an analytical solution of $T_k(r)$, $J_k(\gamma_2\,\sigma^2)$ is developed as a Zernike $2k$-series[6,12,13] in order to obtain a solution in the general case :

$$J_k(\gamma_2\,\sigma^2) = \sum_{p=0}^{\infty} \beta_{2k+2p}^{2k}(\gamma_2) R_{2k+2p}^{2k}(\sigma). \tag{A1}$$

Here $\beta_{2k+2p}^{2k}(\gamma_2)$ equals the decomposition coefficient and $R_{2k+2p}^{2k}(\sigma)$ equals the basis function of decomposition (Zernike polynomial). The mathematical expression for the coefficients is:

$$\beta_{2k+2p}^{2k}(\gamma_2) = 2(2k+2p+1)\int_0^1 J_k(\gamma_2\,\sigma^2) R_{2k+2p}^{2k}(\sigma)\sigma\, d\sigma. \tag{A2}$$

The factor $2(2k+2p+1)$ in front of the previous integral allows us to normalize the coefficients. By taking into account the Eqs. (17) and (A2) and by introducing them in Eq. (16), we obtain :

$$T_k(r) = \sum_{p=0}^{\infty} \beta_{2k+2p}^{2k}(\gamma_2) V_{2k+2p}^{2k}(r,u), \tag{A3}$$

where

$$V_{2k+2p}^{2k}(r,u) = \int_0^1 \exp\left(i\frac{1}{2}u\sigma^2\right) R_{2k+2p}^{2k}(\sigma) J_{2k}\left(\frac{\pi d}{\lambda z} r\sigma\right) \sigma d\sigma. \tag{A4}$$

The V_{2k+2p}^{2k} can be evaluated by means of a digital computation scheme.[12,13] Its development is based on the the recent extension of the Nijboer-Zernike approach in terms of Bessel-Bessel series expression by linearization of Zernike polynomials products. The Bessel-Bessel series expression for V_{2k+2p}^{2k} is :

$$V_{2k+2p}^{2k}(r,u) = \exp\left(i\frac{u}{4}\right) \sum_{m=0}^{\infty} (2m+1) i^m j_m\left(\frac{u}{4}\right) \sum_{l=\max(0,m-2k-p,p-m)}^{m+p} (-1)^l \omega_{ml} \frac{J_{2k+2l+1}\left(\frac{\pi d}{\lambda z} r\right)}{\left(\frac{\pi d}{\lambda z} r\right)}. \tag{A5}$$

All coefficients are defined in the Appendix B. These series allow us to apply our method in the future for cases where $|u|$ may be much larger. Now, it is possible to give a series expression for the decomposition coefficient $\beta_{2k+2p}^{2k}(\gamma_2)$. To do this, it is necessary to recall that:[1]

$$J_k(\gamma_2\,\sigma^2) = \left(\frac{1}{2}\gamma_2\,\sigma^2\right)^k \sum_{s=0}^{\infty} \frac{\left(\frac{1}{2} i \gamma_2 \sigma^2\right)^{2s}}{s!(k+s)!}, \tag{A6}$$

Equation (A6) is introduced in Eq. (A2) and by changing the integral and the sum symbols, we can write:

$$\beta_{2k+2p}^{2k}(\gamma_2) = 2(2k+2p+1)\left(\frac{1}{2}\gamma_2\right)^k \sum_{s=0}^{\infty} \frac{\left(\frac{1}{2} i \gamma_2\right)^{2s}}{s!(k+s)!} \int_0^1 \sigma^{2k+4s} R_{2k+2p}^{2k}(\sigma)\sigma d\sigma. \tag{A7}$$

Next we use the following relationship proposed in Ref.[12] and proved in Ref.,[6] Appendix A :

$$\int_0^1 \sigma^{2k+4s} R^{2k}_{2k+2p}(\sigma)\sigma d\sigma = \frac{1}{2}(-1)^p \frac{(-2s)_p}{(2k+2s+1)_{p+1}}, \tag{A8}$$

where $(q)_n$ denotes the shifted factorial defined by $q(q+1)(q+2)\dots(q+n-1)$ for $n>0$, $(q)_0=1$. Note that $(-2s)_p = 0$ for $0 \le 2s < p-1$. So the decomposition coefficients are

$$\beta^{2k}_{2k+2p}(\gamma_2) = 2(2k+2p+1)\left(\frac{1}{2}\gamma_2\right)^k \sum_{s=r}^{\infty} \frac{\left(\frac{1}{2}i\gamma_2\right)^{2s}}{s!(k+s)!}\ \frac{1}{2}\frac{(-1)^p(-2s)_p}{(2k+2s+1)_{p+1}}. \tag{A9}$$

The variable r is the first integer $\ge \frac{1}{2}p$. We can now write $j = s-r$ so that the previous expression becomes

$$\beta^{2k}_{2k+2p}(\gamma_2) = (2k+2p+1)(-1)^r \left(\frac{1}{2}\gamma_2\right)^{k+2r} \sum_{j=0}^{\infty} \kappa_j \frac{\left(-\frac{1}{4}\gamma_2^2\right)^j}{j!} \tag{A10}$$

with

$$\kappa_j = \frac{j!}{(j+r)!(k+j+r)!}\ \frac{(-1)^p(-2j-2r)_p}{(2k+2j+2r+1)_{p+1}}. \tag{A11}$$

The coefficients of $\left(\frac{1}{2}i\gamma_2\right)^{2j}$ are rational functions of j whence it is possible to express (A10) in terms of hypergeometric functions[1,4] by considering two cases: $2r-p=0$ and $2r-p=1$. In the case $2r-p=0$ one obtains :

$$\beta^{2k}_{2k+2p}(\gamma_2) = d_0^0\,(-1)^r(2k+4r+1)\left(\frac{1}{2}\gamma_2\right)^{k+2r} {}_2F_3\left(\begin{matrix} r+\frac{1}{2} & k+r+\frac{1}{2} \\ \frac{1}{2} & k+2r+\frac{3}{2} \quad k+2r+1 \end{matrix}; -\frac{1}{4}\gamma_2^2\right). \tag{A12}$$

In the case $2r-p=1$, one obtains:

$$\beta^{2k}_{2k+2p}(\gamma_2) = d_0^1\,(-1)^r(2k+4r-1)\left(\frac{1}{2}\gamma_2\right)^{k+2r} {}_2F_3\left(\begin{matrix} r+\frac{1}{2} & k+r+\frac{1}{2} \\ \frac{3}{2} & k+2r+1 \quad k+2r+\frac{1}{2} \end{matrix}; -\frac{1}{4}\gamma_2^2\right). \tag{A13}$$

In Eq. (A12) and (A13) , the coefficients d_0^0 and d_0^1 are defined as follows:

$$d_0^0 = \frac{(2r)!(2k+2r)!}{r!(k+r)!(2k+4r+1)!} \qquad d_0^1 = \frac{(2r)!(2k+2r)!}{r!(k+r)!(2k+4r)!}. \tag{A14}$$

B Appendix B : Coefficients of the Bessel-Bessel series expansion for V_{2k+2p}^{2k}

The quantities occuring in the series expression for V_{2k+2p}^{2k}, see Eq. (A5), are given as:

$$
\begin{aligned}
\omega_{ml} &= \sum_{s=0}^{p} \sum_{t=0}^{\min(m,s)} f_{ps}^{2k} b_{mst} g_{m+s-2t,l}^{2k}, \\
f_{ps}^{2k} &= (-1)^{p-s} \frac{2s+1}{p+s+1} \frac{\begin{pmatrix} 2k+p-s-1 \\ 2k-1 \end{pmatrix} \begin{pmatrix} 2k+p+s \\ s \end{pmatrix}}{\begin{pmatrix} p+s \\ s \end{pmatrix}}, \qquad s = 0, \ldots, p, \\
g_{ul}^{2k} &= \frac{2k+2l+1}{2k+u+l+1} \frac{\begin{pmatrix} 2k \\ u-l \end{pmatrix} \begin{pmatrix} u+l \\ l \end{pmatrix}}{\begin{pmatrix} 2k+l+u \\ 2k+l \end{pmatrix}}, \qquad u = l, \ldots, l+2k, \qquad s_1, s_2 = 0, 1, \ldots, \\
b_{s_1 s_2 t} &= \frac{2s_1 + 2s_2 - 4t + 1}{2s_1 + 2s_2 - 2t + 1} \frac{A_{s_1 - t} A_t A_{s_2 - t}}{A_{s_1 + s_2 - t}}, \qquad t = 0, \ldots, \min(s_1, s_2), \\
A_m &= \begin{pmatrix} 2m \\ m \end{pmatrix}.
\end{aligned}
\tag{B1}
$$

The spherical Bessel function $j_r(z)$ is defined by

$$
j_r(z) = \sqrt{\frac{\pi}{2z}}\, J_{r+\frac{1}{2}}(z) \tag{B2}
$$

Acknowledgments

The authors thanks his colleagues Dr. P. Dirksen from Philips Reseach Leuven for passing his software programs to compute the integrals in Eq. (A5)

References

1. Abramowitz and Stegun, Handbook of Mathematical Functions, *Dover Publications, Inc., New York*, (1970).

2. Tatiana Alieva and Maria Luisa Calvo, "Importance of the phase amplitude in the fractional Fourier domain", J. Opt. Soc. Am. A **20**, 533-541 (2003).

3. Anderson W.L. and Hongyan Diao, "Two dimensional wavelet transform and application to holographic particle velocimetry", Appl. Opt. **34**, 249–255 (1995).

4. G. E. Andrews, R. Askey, and R. Roy, Special Functions, *Cambridge University Press*, (1999).

5. M. Born and E. Wolf, Principles of Optics, *Cambridge University Press,* 7^e *ed.*, (1999).

6. J.J.M. Braat, P. Dirksen and A.J.E.M. Janssen, "Assessment of an extended Nijboer-Zernike approach for the computation of optical point-spread functions", J. Opt. Soc. Am. A **19**, 858–870 (2002).

7. C. Buraga, S. Coëtmellec, D. Lebrun and C. Özkul, " Application of wavelet transform to hologram analysis: three-dimensional location of particles ", Opt. And Lasers Eng. **33**, 409–421(2000).

8. Yangjian Cai and Qiang Lin, "Propagation of elliptical Gaussian beam through misaligned optical systems in spatial domain and frequency domain", Optics and Laser Techonoloy, **34**, 415–421 (2002).

9. Yangjian Cai and Qiang Lin, "Fractional Fourier transform for elliptical Gaussian beams", Opt. Comm., **217**, 7–13, (2003).

10. S. Coëtmellec, D. Lebrun and C. Özkul, "Application of the two-dimensional fractional-order Fourier transformation to particle field digital holography", J. Opt. Soc. Am. A **19**, 1537–1546 (2002).

11. M. Gustafsson, M. Sebesta, B.Bengtsson, S.G. Pettersson, P. Egelberg and T. Lenart, " High-resolution digital transmission microscopy - a Fourier holography approach", Opt. And Lasers Eng. **41**, 553–563(2004).

12. A.J.E.M. Janssen, "Extended Nijboer-Zernike approach for the computation of optical point-spread functions", J. Opt. Soc. Am. A **19**, 849-857 (2002).

13. A.J.E.M. Janssen, J.J.M. Braat and P. Dirksen, "On the computation of the Nijboer-Zernike aberration integrals at arbitrary defocus ", J. Mod. Optics, **51**, n°5, 687–703 (2004).

14. T. M. Kreis and W. P. O. Jüptner " Suppression of the dc term in digital holography", Opt. Eng. **36**, 2357–2360 (1997).

15. A. W. Lohmann , " Image rotation, Wigner rotation, and the fractional Fourier transform", J. Opt. Soc. Am. A **10**, 2181–2186 (1993).

16. A.C. McBride and F.H. Kerr, " On Namias's Fractional Fourier Transforms", IMA J. Appl. Math. **39**, 159–175 (1987).

17. D. Mendlovic, M. Ozaktas and A. W. Lohmann, "Graded-index fibers, Wigner-distribution functions, and the fractional Fourier transform", Appl. Opt. **33**, 6188–6193 (1994).

18. V. Namias, " The fractional Order Fourier Transform and its Application to quantum Mechanics", J. Inst. Maths Its Applics, **25**, 241–265 (1980).

19. L. Onural, " Diffraction from a wavelet point a view", Opt. Lett. **18**, 846–848 (1993).

20. H. Ozaktas and D. Mendlovic, "Fractional Fourier optics", J. Opt. Soc. Am. A **12**, 743-751 (1995).

21. Soo-Chang Pei and Jian-Jiun Ding, " Closed-form discrete fractional and affine Fourier transforms", IEEE Trans.

Signal Process. **17**, 1338-1353 (2000).

22. P. Pellat-Finet, "Fresnel diffraction and the fractional-order Fourier transform", Opt. Lett. **19**, 1388-1390 (1994).

23. P. Pellat-Finet, "Diffraction entre un émetteur et un récepteur localement toriques. Application à l'étude des systèmes astigmates", C.R. Acad. Sci. Paris, t.327, Série IIb, 1269–1274 (1999).

24. Chandra S. Vikram and Michael L. Billet "Gaussian beam effects in far-field in-line holography", Appl. Opt. **22**, 2830–2835 (1983).

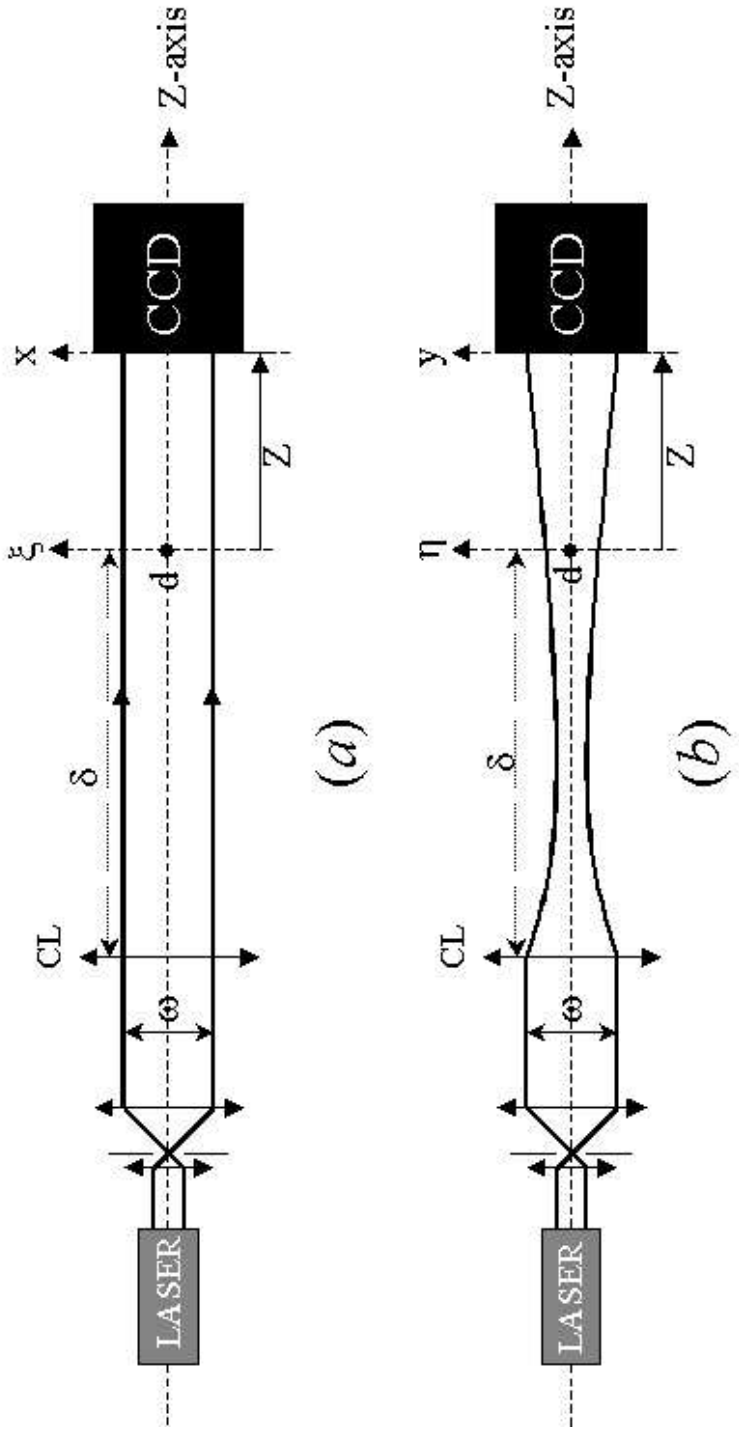

Fig. 1. Experimental optical set-up.

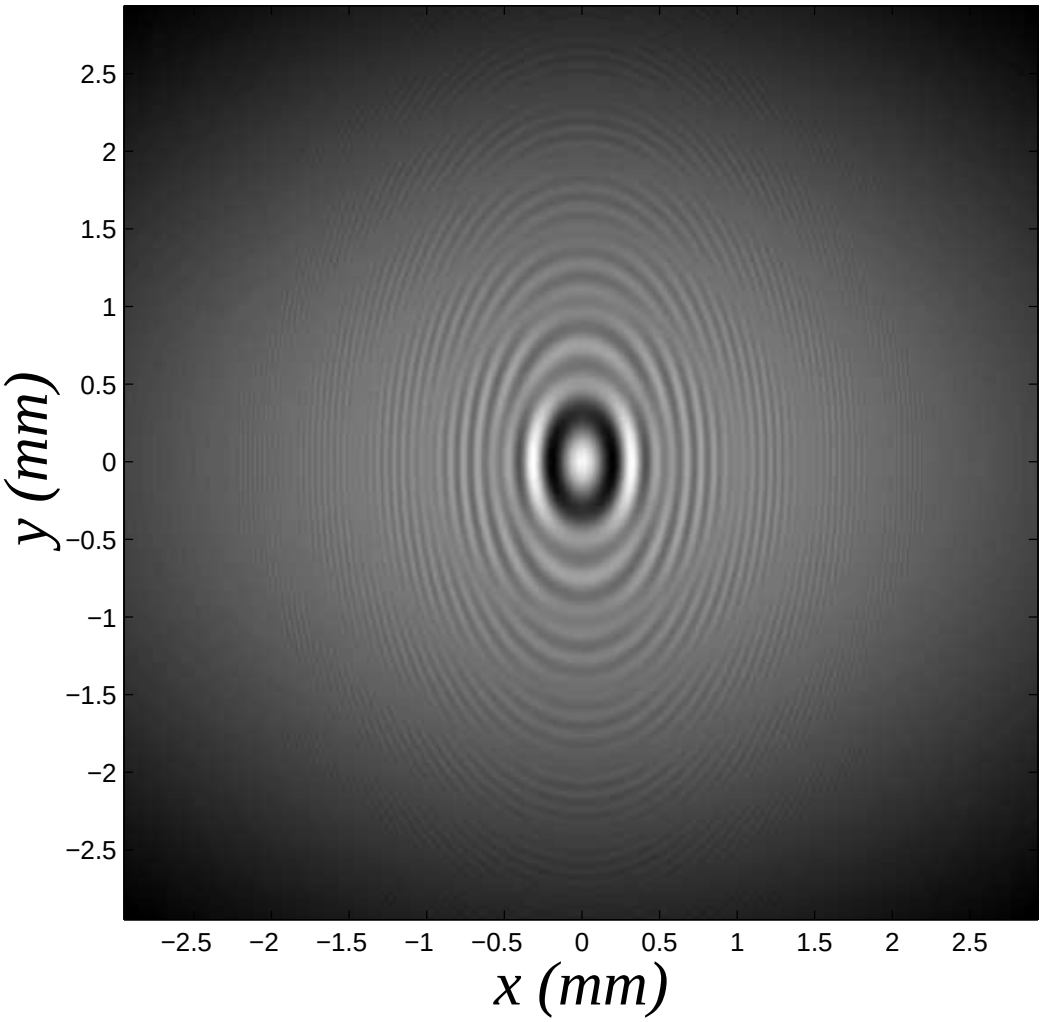

Fig. 2. Diffraction pattern with $\lambda = 632.8nm$, $\omega_\xi = 7mm$, $\omega_\eta = 1.75mm$, $R_\xi = -2.36 \cdot 10^5 m$, $R_\eta = -50mm$, $d = 150\mu m$ and $z = 107mm$

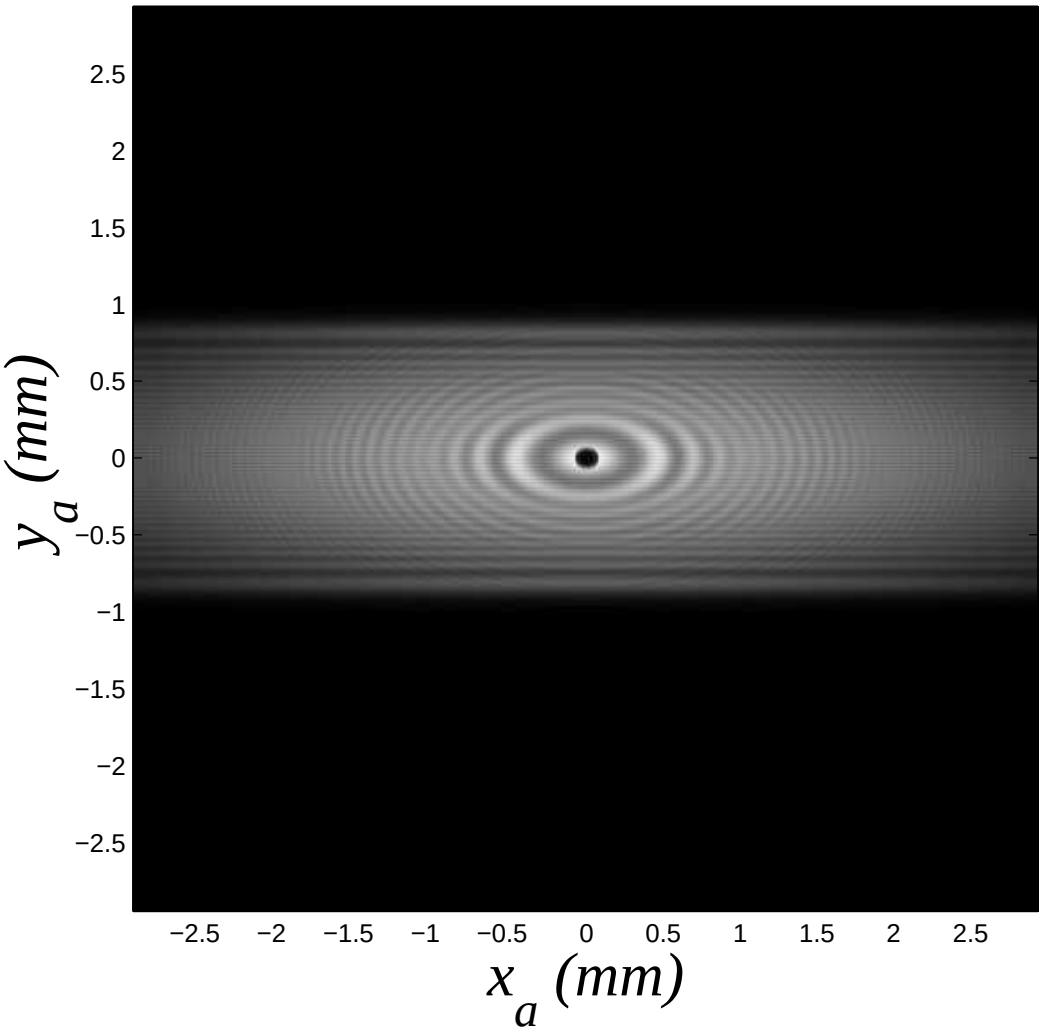

Fig. 3. Image reconstructed by the fractional Fourier transformation with $a_x^{opt} = 0.521$ and $a_y^{opt} = 0.816$

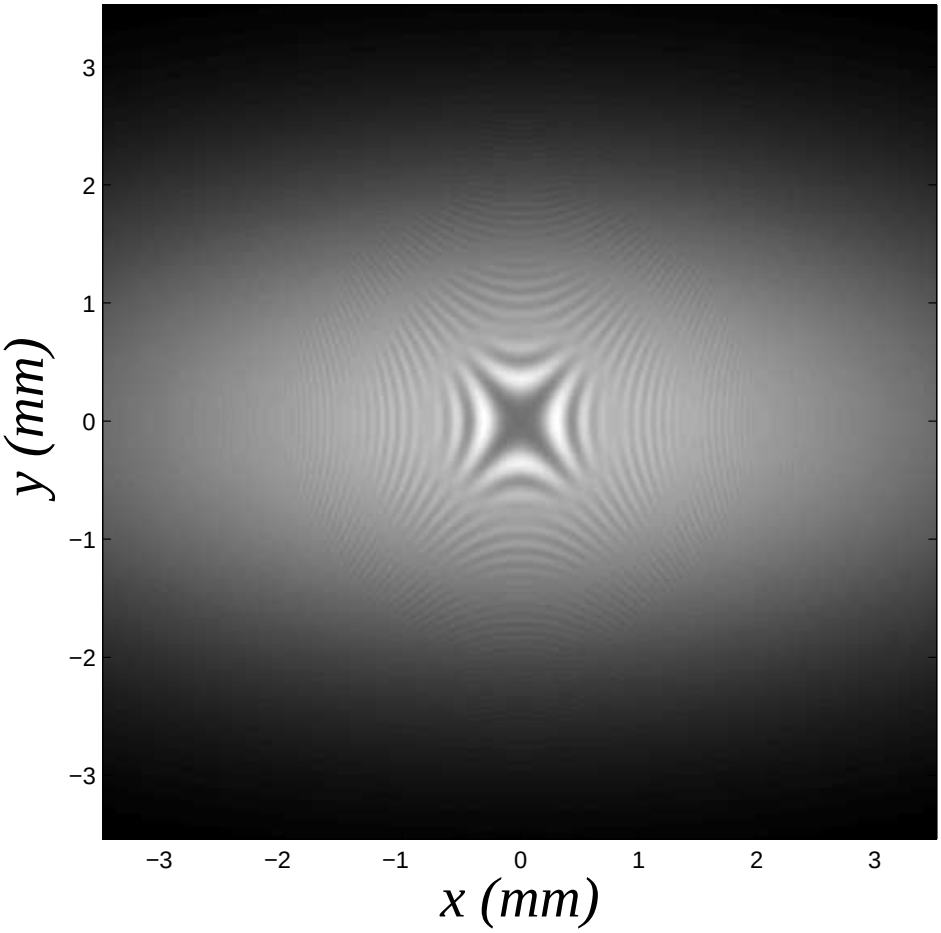

Fig. 4. Diffraction pattern with $\lambda = 632.8nm$, $\omega_\xi = 7mm$, $\omega_\eta = 2.27mm$, $R_\xi = -4.38 \cdot 10^5 m$, $R_\eta = 65mm$, $d = 150\mu m$ and $z = 154mm$

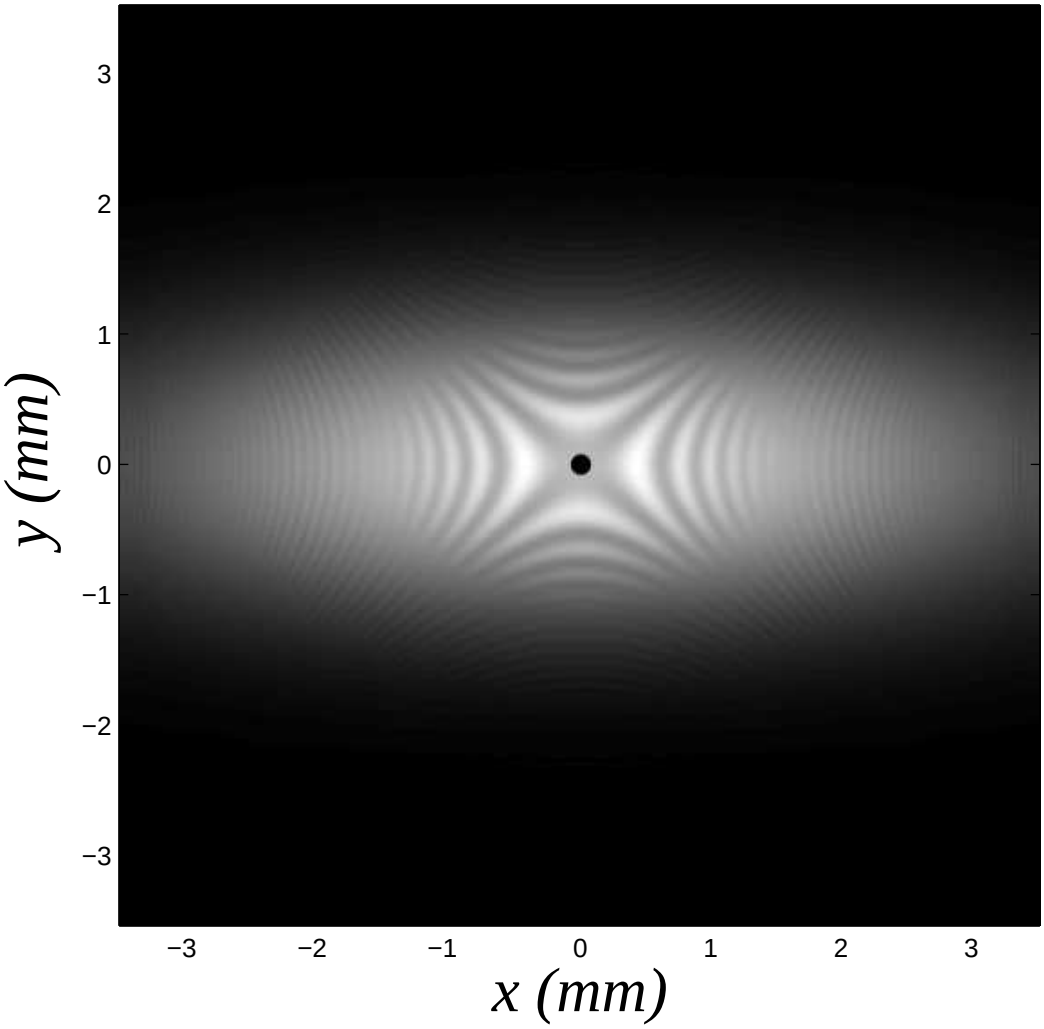

Fig. 5. Image reconstructed by the fractional Fourier transformation with $a_x^{opt} = 0.633$ and $a_y^{opt} = -0.718$

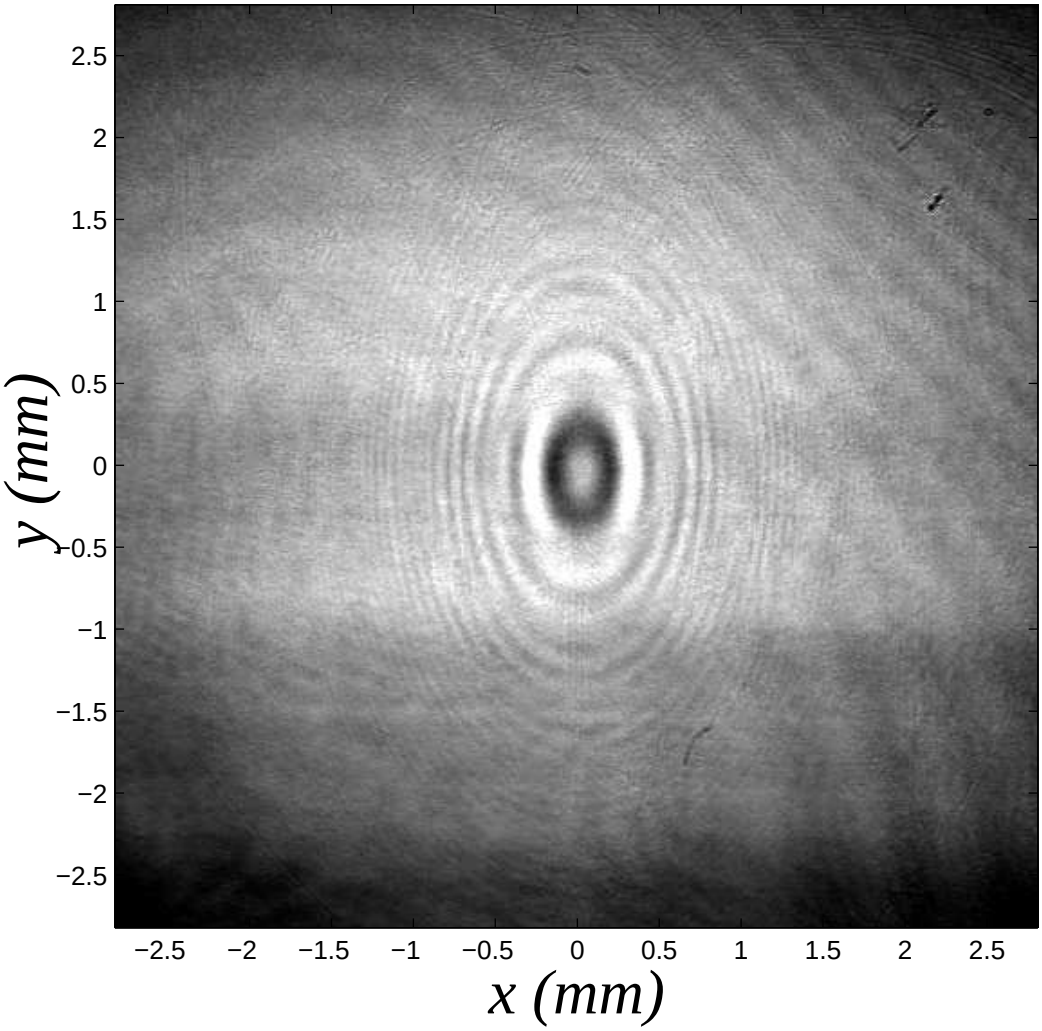

Fig. 6. Diffraction pattern with $\lambda = 632.8nm$, $\omega_\xi = 7mm$, $\omega_\eta = 1.75mm$ $R_\xi = -2.36 \cdot 10^5 m$, $R_\eta = -50mm$, $d = 150\mu m$ and $z = 106mm$

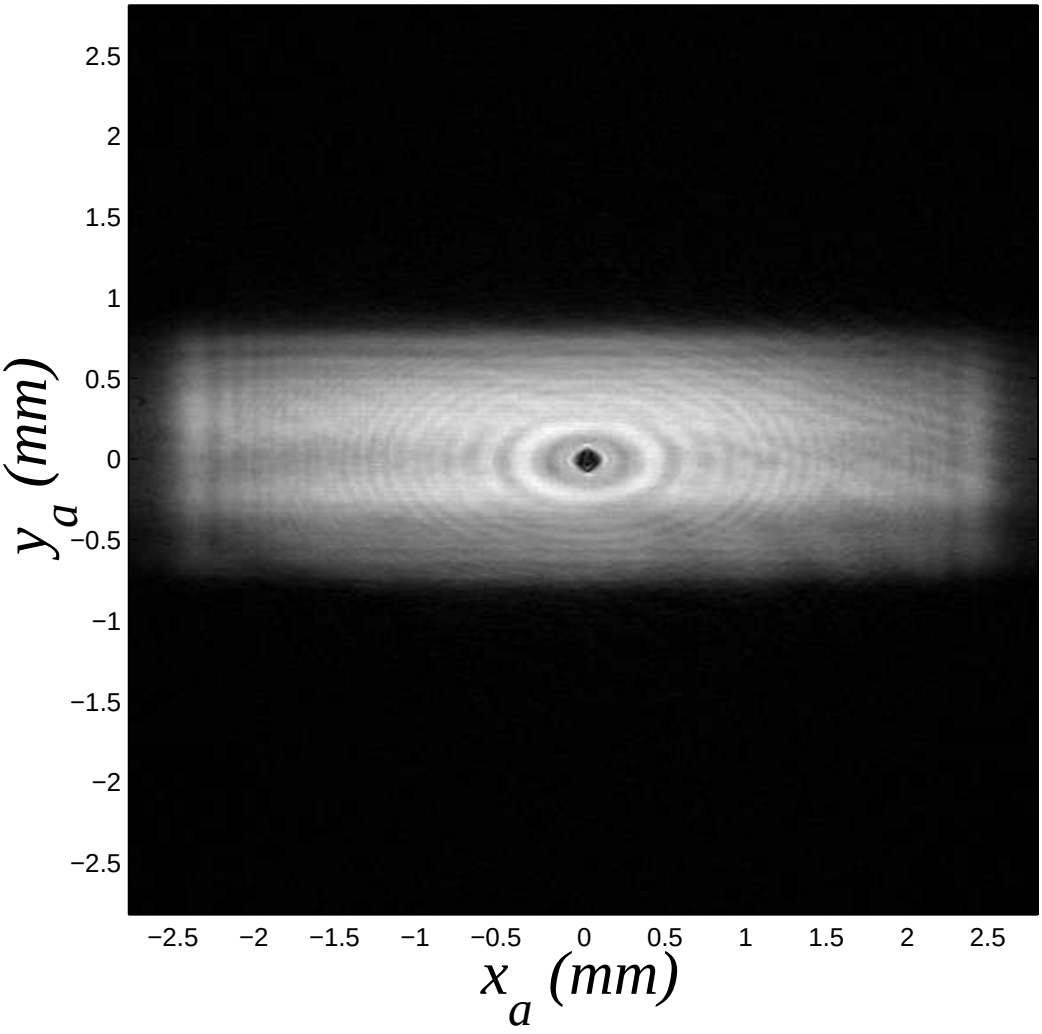

Fig. 7. Image reconstructed by the fractional Fourier transformation with $a_x^{opt} = 0.518$ and $a_y^{opt} = 0.813$

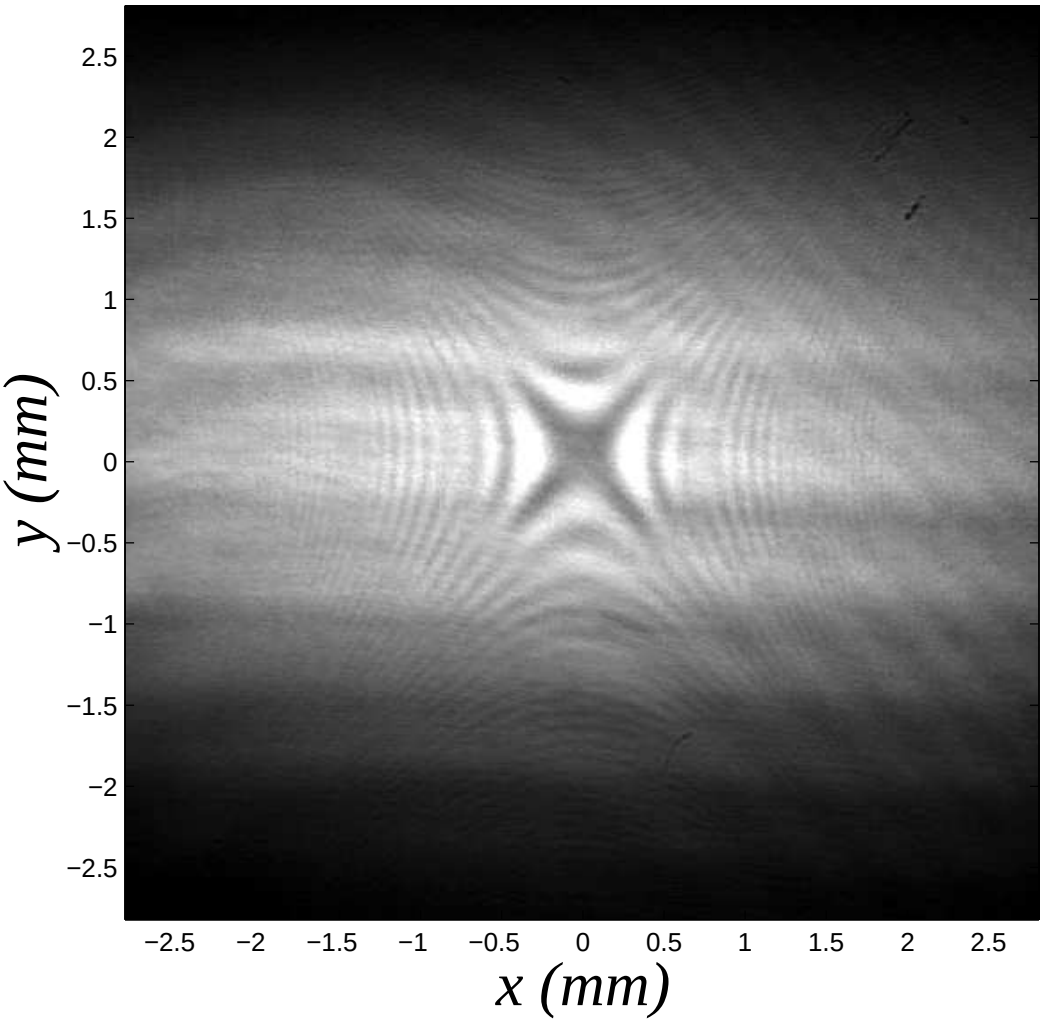

Fig. 8. Diffraction pattern with $\lambda = 632.8nm$, $\omega_\xi = 7mm$, $\omega_\eta = 2.27mm$, $R_\xi = -4.38 \cdot 10^5 m$, $R_\eta = 65mm$, $d = 150\mu m$ and $z = 154mm$

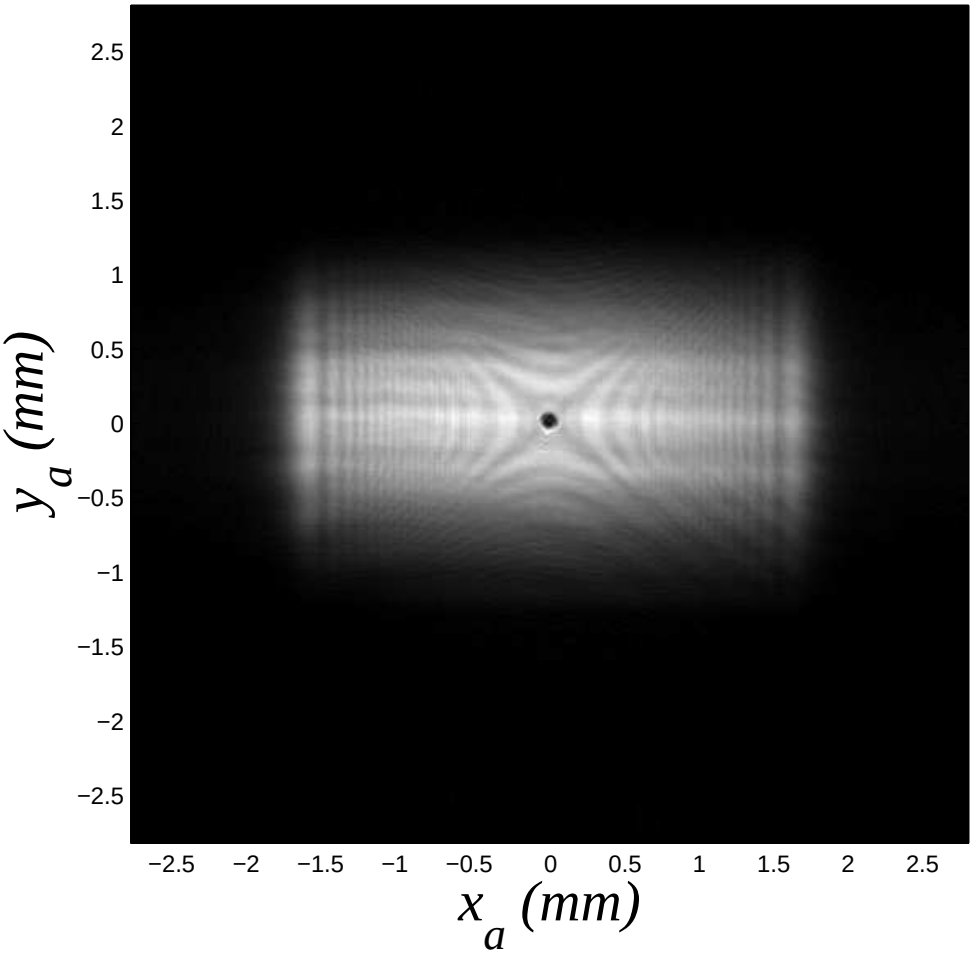

Fig. 9. Image reconstructed by the fractional Fourier transformation with $a_x^{opt} = 0.633$ and $a_y^{opt} = -0.718$